THE JOURNAL OF PHYSICAL CHEMISTRY C

Article

Cite This: J. Phys. Chem. C 2018, 122, 8998−9008

pubs.acs.org/JPCC

In Situ Characterization of Mesoporous Co/CeO_2 Catalysts for the High-Temperature Water-Gas Shift

Dimitriy Vovchok,[†,§] Curtis J. Guild,[⊥] Shanka Dissanayake,[⊥] Jordi Llorca,[#] Eli Stavitski,[†,∥] Zongyuan Liu,[§] Robert M. Palomino,[†] Iradwikanari Waluyo,[∥] Yuanyuan Li,[‡] Anatoly I. Frenkel,[‡,§] José A. Rodriguez,[†,§] Steven L. Suib,*[,⊥] and Sanjaya D. Senanayake*[,§]

[†]Department of Chemistry and [‡]Department of Materials Science and Chemical Engineering, Stony Brook University, Stony Brook, New York 11794, United States

[§]Chemistry Department and [∥]National Synchrotron Light Source II, Brookhaven National Laboratory, Upton, New York 11973, United States

[⊥]Department of Chemistry, University of Connecticut, 55 N. Eagleville Rd., Storrs, Connecticut 06269, United States

[#]Institute of Energy Technologies, Department of Chemical Engineering and Barcelona Research Center in Multiscale Science and Engineering, Technical University of Catalonia, Barcelona 08019, Spain

Supporting Information

ABSTRACT: Mesoporous Co/CeO_2 catalysts were found to exhibit significant activity for the high-temperature water-gas shift (WGS) reaction with cobalt loadings as low as 1 wt %. The catalysts feature a uniform dispersion of cobalt within the CeO_2 fluorite type lattice with no evidence of discrete cobalt phase segregation. *In situ* XANES and ambient pressure XPS experiments were used to elucidate the active state of the catalysts as partially reduced cerium oxide doped with oxidized cobalt atoms. *In situ* XRD and DRIFTS experiments suggest facile cerium reduction and oxygen vacancy formation, particularly with lower cobalt loadings. *In situ* DRIFTS analysis also revealed the presence of surface carbonate and bidentate formate species under reaction conditions, which may be associated with additional mechanistic pathways for the WGS reaction. Deactivation behavior was observed with higher cobalt loadings. XANES data suggest the formation of small metallic cobalt clusters at temperatures above 400 °C may be responsible. Notably, this deactivation was not observed for the 1% cobalt loaded catalyst, which exhibited the highest activity per unit of cobalt.

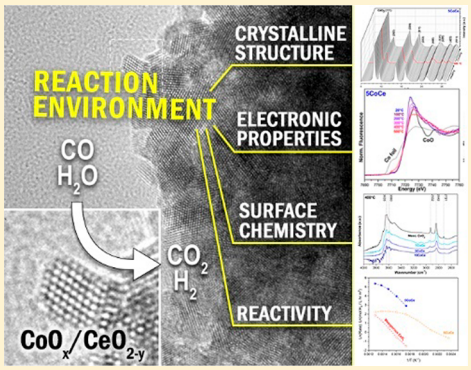

INTRODUCTION

Production of pure hydrogen gas for renewable fuel and chemical synthesis applications remains an area of significant research interest. Currently, over 95% of the world's hydrogen supply is produced through the reforming of fossil fuels.[1] This reforming process necessarily generates a product stream (reformate gas or syngas[2]) with a significant concentration of carbon monoxide. The CO content is highly detrimental to the application of hydrogen toward synthesis processes and hydrogen fuel cells, since CO acts as a catalyst poisoning agent.[3] For this reason, the removal of CO from reformate gas feeds is necessitated as a part of the hydrogen generation process.

The water-gas shift (WGS: $CO_{(g)} + H_2O_{(g)} \rightleftharpoons CO_{2(g)} + H_{2(g)}$, $\Delta H = -41$ kJ mol^{-1}) reaction[4] is widely applied to industrial hydrogen generation processes in order to remove CO from reformate gas and generate additional hydrogen product.[5] The WGS is typically carried out with the help of heterogeneous catalyst materials in two temperature stages in order to take advantage of both kinetic and thermodynamic properties of the mildly exothermic reaction.[6,7] The high-temperature stage (HT-WGS) is typically carried out at between 350 and 450 °C, although in some cases this temperature can be as high as 600 °C.[8,9] Ferrochrome[10] and other iron-based catalysts[11,12] are commonly used for the HT-WGS reaction.

Well-dispersed metals supported on cerium oxide have been frequently studied as catalysts for both low- and high-temperature water-gas shift reactions.[13−15] Cerium oxide is often considered an active catalytic support material due to its excellent reducibility and oxygen transport properties[16−18] and strong metal−support interactions.[19] Oxygen vacancy sites present in partially reduced ($Ce^{4+} \rightarrow Ce^{3+}$) cerium oxide have been identified as playing a role in the dissociation of water during the WGS reaction,[20,21] while supported metal particles account for the adsorption and activation of the CO molecule. Additionally, an associative WGS reaction pathway is available on the surface of these materials through the formation of

Received: February 5, 2018
Revised: April 4, 2018
Published: April 4, 2018

DOI: 10.1021/acs.jpcc.8b01271
J. Phys. Chem. C 2018, 122, 8998−9008

H_xCO_y intermediate species such as formates, carbonates, and carboxyls.[22]

In recent years, a novel sol−gel synthesis technique was developed to produce a highly crystalline, monodisperse, and mesoporous CeO_2 morphology.[23] The resulting material demonstrated significant activity for the WGS reaction as a stand-alone, metal-free catalyst.[24] In a subsequent study, we have successfully synthesized and evaluated the activity and unique metal−support interactions of copper-loaded mesoporous CeO_2 catalysts for the low-temperature WGS reaction.[25] Building upon this work, we have synthesized mesoporous Co/CeO_2 materials with Co loadings between 1% and 10% as potential catalysts for the high-temperature WGS reaction. Relatively high loading (15%−35%) Co/CeO_2 catalysts have been reported as active for the HT-WGS in recent studies,[26,27] with activity being attributed to strong metal−support interactions enhancing a segregated Co_3O_4 phase, which is known to have significant CO oxidation capabilities.[28] Particularly, the importance of Co^{2+} in the WGS reaction has been proposed and reported in several past studies.[29−31] In this study, we examine mesoporous Co/CeO_2 materials that do not exhibit an observable segregated cobalt oxide phase and demonstrate significant catalytic activity for the HT-WGS reaction with low loadings of cobalt. In our catalysts, small clusters or atoms of cobalt are embedded into the mesoporous ceria preventing the typical chemistry seen for bulk Co, avoiding C−O bond breaking and Fischer−Tropsch catalysis.

EXPERIMENTAL SECTION

Catalyst Synthesis. Mesoporous cobalt-doped CeO_2 catalysts were synthesized using the sol−gel synthesis method.[23] For the synthesis of 1% Co/CeO_2 catalysts, 8.7 g of $Ce(NO_3)_3{\cdot}6H_2O$, 0.059 g of $Co(NO_3)_2{\cdot}6H_2O$, 3 g of Pluronic-P-123, and 1.5 mL of nitric acid were mixed in 1.5 mL of 1-butanol at 60 °C to form a homogeneous solution. The solution was heated in a ventilated oven at 120 °C for about 2.5 h. The products were cooled, washed in excess ethanol, and dried under vacuum overnight. The solids were then loaded into alumina crucibles and heated to the calcination temperature of 450 °C with a ramp rate of 5 °C/min. The samples were kept at 450 °C for 4 h. Higher cobalt loadings (5% and 10%) were prepared using the same procedure except with 5% and 10% molar ratios of cobalt to cerium. For the purposes of this study, the 1%, 5%, and 10% mesoporous Co/CeO_2 materials will be abbreviated as **1CoCe**, **5CoCe**, and **10CoCe**, respectively.

Transmission Electron Microscopy. High-resolution transmission electron microscopy (HRTEM) and scanning transmission electron microscopy (STEM-HAADF-EDX) characterization was carried out at the Technical University of Catalonia using a Tecnai G2 F20 S-TWIN microscope equipped with a field emission electron source and operated at 200 kV. Samples were dispersed in alcohol suspension and supported on holey carbon film over the grid.

Textural Studies. N_2 sorption experiments on the mesoporous ceria were performed with a Quantachrome Autosorb-1-1C automated sorption system. All the samples were degassed at 150 °C for 6 h under vacuum prior to measurement. The surface areas were calculated using the Brunauer−Emmett−Teller (BET) method, and pore sizes and volumes were calculated from the desorption branch of the isotherm using the Barrett−Joyner−Halenda (BJH) method.

Catalytic Activity Studies. The catalytic activity was evaluated in a home-built horizontal fixed-bed reactor equipped with a gas manifold and a standardized process gas chromatograph (GC, SRI International Multigas #2) for sampling the outlet gas. About 50 mg of catalyst was packed into a quartz reactor and supported by quartz wool. Catalyst materials were not sieved for particle size. The catalyst was cleaned under flowing helium at 200 °C for an hour, cooled to room temperature, and then exposed to the WGS conditions (5% CO, 3% H_2O, balance He) at 9500 h^{-1} GHSV. The catalyst was then ramped to 300 °C, and measurements were taken in 50 °C increments up to 500 °C. At each temperature, three data points were taken.

X-ray Photoelectron Spectroscopy (XPS). Ambient pressure XPS measurements were carried out at Brookhaven National Laboratory (BNL). Powder sample was pressed into an aluminum plate and introduced into an ultrahigh-vacuum environment, where a conventional Mg X-ray source was used to probe the material. Ambient pressure measurements were collected after introducing 25 mTorr of CO and 25 mTorr of H_2O into the chamber and heating the sample stepwise to 100, 200, and 400 °C. The Ce 3d region was plotted and analyzed using CasaXPS software.[32]

***In Situ* Synchrotron X-ray Diffraction (XRD).** *In situ* X-ray diffraction (XRD) experiments detailed in this study were performed at Advanced Photon Source (APS) in Argonne National Laboratory at beamline 17BM-B. The experiments were carried out using the Clausen[33] capillary flow reactor. A quartz capillary with an inner diameter of 0.9 mm and outer diameter of 1.1 mm was loaded with approximately 5 mg of sample between two segments of quartz wool. Reactant gas consists of 5% CO (in helium) flown through a room temperature water bubbler to achieve 3% H_2O concentration. The reactant gas mixture is flown continuously through the capillary at a rate of 10 cm^3/min. The temperature of the reactor cell is controlled using a controlled resistance heating coil. The temperature profile for the experiments consisted of stepwise heating and cooling up to 400 °C. X-ray diffraction patterns are collected continuously during the experiment. Outflow gas during XRD experiments was analyzed using a residual gas analyzer (RGA)−quadrupole mass spectrometry unit in order to provide a qualitative WGS activity analysis by monitoring the production of H_2 and CO_2 gas. The X-ray wavelength utilized for XRD was either 0.727 68 or 0.453 36 Å, depending on sample, since the data sets were collected over the course of several scheduling intervals with different beamline configurations. X-ray diffraction patterns were plotted in Origin and processed using the GSAS II software[34] to obtain structural information via Rietveld refinement.[35]

X-ray Absorption Spectroscopy (XAS). *In situ* Co K-edge X-ray absorption near-edge structure (XANES) measurements were carried out under WGS reaction environment conditions (5% CO, 3% H_2O, balance He) at beamline 8-ID (ISS) at the National Synchrotron Light Source II (NSLS-II) at Brookhaven National Laboratory, which is a high flux (10^{14} ph/sec at 10 keV) wiggler spectroscopy beamline equipped with a Si 111 double crystal high heat load monochromator. An identical reaction cell environment was used as described for X-ray diffraction experiments. The reaction cell was heated stepwise, and XANES measurements were collected at 20, 100, 200, 300, 400, and 500 °C using an array of silicon drift fluorescence detectors.

DOI: 10.1021/acs.jpcc.8b01271
J. Phys. Chem. C 2018, 122, 8998−9008

Ex situ Co K-edge extended X-ray absorption fine structure (EXAFS) measurements were also carried out at beamlines 8-ID (ISS) at NSLS-II and 20-ID at APS in fluorescence detection mode. Near-edge X-ray absorption fine structure (NEXAFS) spectra (Co $L_{2,3}$-edge and Ce $M_{4,5}$-edge) were collected in total electron yield (TEY) mode at beamline 23-ID-2 (IOS) at NSLS II. All X-ray absorption data were processed using the Athena software.[36] For the purposes of this study, the term XANES is used to refer to hard X-ray experiments, and the equivalent term NEXAFS is used to refer to soft X-ray experiments.

The XANES spectra were calculated theoretically using FEFF 9 code.[37] Simulations were first performed on CoO for finding optimized conditions for FEFF calculations. For all calculations, identical parameters were used to account for experimental broadening in all spectra that were all measured using the same experimental setups. XANES simulation was performed for two models. In the first model (Figure 12b), the Co atom sits above the surface layer of ceria sphere (containing 191 atoms) with four nearest oxygen atoms at the distance of 2.13 Å (as in CoO). In the second model (Figure 12a), Co atom replaces the Ce atom in the center of the ceria sphere. The model for ceria was obtained by putting a Ce atom in the center of the sphere with the cutoff distance of 8.1 Å.

Diffuse Reflectance Infrared Fourier Transform Spectroscopy (DRIFTS). DRIFTS experiments were performed at the Advanced Energy Center (AERTC) at Stony Brook University. The reactor cell was loaded with sample material and heated to 100 °C, followed by stepwise heating in 100 °C increments up to 500 °C under WGS reaction environment conditions (5% CO, 3% H_2O, balance He). Infrared spectra (4000−600 cm^{-1}) were recorded every 85 s. KBr background was subtracted from all spectra. Data were processed using Thermo Scientific OMNIC 8 software.

RESULTS AND DISCUSSION

Morphology and Texture. A transmission electron microscopy study was carried out to examine the local morphology of mesoporous Co/CeO_2 samples with cobalt loadings of 1% (**1CoCe**), 5% (**5CoCe**), and 10% (**10CoCe**). Representative images of **10CoCe** are reported in Figure 1. The **10CoCe** material was found to consist of highly crystalline, monodisperse nanoparticles measuring 4.0 ± 0.5 nm in diameter. A selected area electron diffraction (SAED) pattern recorded over hundreds of particles indicates a face-centered cubic (fcc) polycrystalline phase with a lattice parameter of 5.41 Å, consistent with the CeO_2 fluorite lattice[38] (Figure 1b). Close examination of individual crystallites (Figure 1d) reveals a truncated octahedral morphology that almost exclusively exposes {111} crystallographic planes. A "zigzag" nanostructure resulting from the removal of several atomic rows is present where {100} planes would be expected (black arrows, Figure 1d). The morphology of these crystallites resembles bare mesoporous CeO_2 materials.[24]

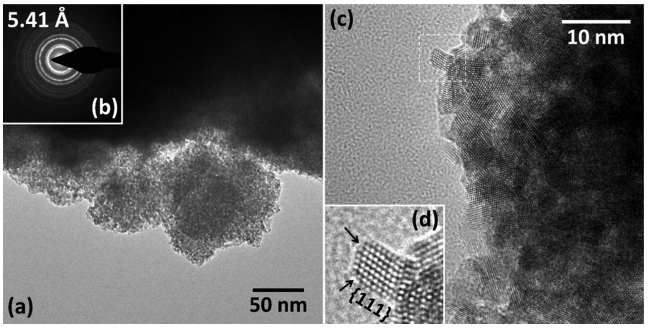

Figure 1. Imaging of **10CoCe** sample: Low-magnification TEM (a), selected area electron diffraction (b), high-resolution TEM (c), and single particle inset (d).

No segregated cobalt content was observed for any mesoporous Co/CeO_2 samples. No crystalline cobalt phases (Co, CoO, Co_2O_3, or Co_3O_4) were indicated on SAED patterns. Likewise, no amorphous content was observed in TEM. However, energy-dispersive X-ray spectroscopy (EDX) measurements indicate the presence of Co in constant proportion with Ce, with a concentration of approximately 9.4% for the **10CoCe** sample (Figure S1). These observations suggest a uniform dispersion of cobalt consistent with a solid solution of cobalt within the CeO_2 fluorite lattice.

TEM imaging of **1CoCe** and **5CoCe** (Figure S2) reveals morphology indistinguishable from the **10CoCe** sample. Particle size analysis and lattice parameters as measured by SAED are indistinguishable from those measured for **10CoCe**.

TEM measurements were also collected for a spent (post-mortem) **10CoCe** sample that has been exposed to water-gas shift (WGS) conditions (5% CO, 3% H_2O, balance He) for 24 h at 400 °C (Figure S3). Following exposure to reaction conditions, particle dispersion and the Co to Ce ratio remained homogeneous throughout the sample. The mean particle size increased slightly to 5 ± 1 nm. Crystallites retained their crystallinity; however, the "zigzag" nanostructure was no longer observed. It is therefore likely that facets other than {111} were exposed under reaction conditions.

Nitrogen adsorption isotherms were measured for mesoporous CeO_2 and mesoporous Co/CeO_2 materials (Figure 2). The surface area according to Brunauer−Emmett−Teller (BET) theory[39] is reported alongside porosity and particle size in Table 1.

The surface areas of mesoporous Co/CeO_2 materials were measured to be significantly smaller than that of bare mesoporous CeO_2 but were not observed to vary significantly between different cobalt loadings. Likewise, the pore volume was measured to be smaller than that of mesoporous CeO_2,

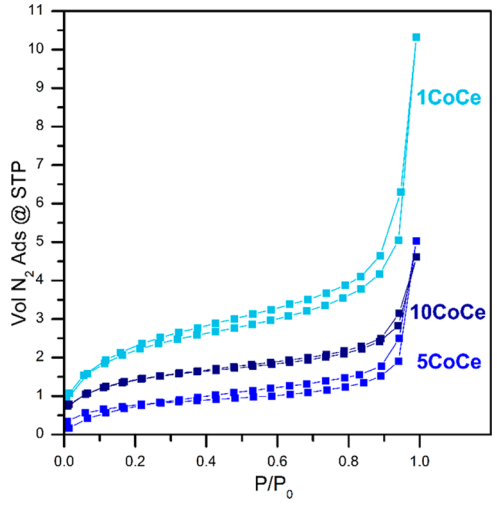

Figure 2. Adsorption isotherms for mesoporous Co/CeO_2 catalysts.

DOI: 10.1021/acs.jpcc.8b01271
J. Phys. Chem. C 2018, 122, 8998−9008

Table 1. Textural and Particle Size Properties of Mesoporous Co/CeO_2 Catalysts

	surface area (m^2 g^{-1})	pore volume (cm^3 g^{-1})	av particle size TEM (nm)
meso CeO_2	163	0.137	3.5
1CoCe	37	0.072	4.0
5CoCe	23	0.065	4.0
10CoCe	34	0.048	4.0

with a slight decreasing trend with increasing cobalt loading. The average particle size for all cobalt containing samples was the same and slightly larger than mesoporous CeO_2.

Spectroscopic Characterization. The electronic and chemical properties of fresh mesoporous Co/CeO_2 catalysts were probed using a combination of near-edge X-ray absorption fine structure (NEXAFS) and X-ray photoelectron spectroscopy (XPS) measurements. Cobalt $L_{2,3}$-edge NEXAFS spectra (Figure 3a) suggest the presence of an oxidized cobalt species in all catalysts. The spectra do not indicate a segregated CoO, Co_2O_3, or Co_3O_4 phase, however. The lack of a key lower energy feature at 777.8 eV indicates the absence of octahedrally coordinated Co^{2+} present in CoO.[40,41] The most intense feature at 780.3 eV may be indicative of octahedrally coordinated Co^{3+} ions.[42] No significant variation was noted between the three cobalt loadings. Additionally, the Co $L_{2,3}$-edge NEXAFS spectra of fresh and spent **10CoCe** samples appear nearly identical, suggesting the chemical state of the cobalt content is recoverable post reaction.

Cerium $M_{4,5}$-edge NEXAFS spectra (Figure 3b) indicate a partially reduced cerium oxide containing both Ce^{3+} and Ce^{4+} ions.[43] No significant differences in the Ce $M_{4,5}$-edge NEXAFS were observed between the three cobalt loadings. The cerium edges of fresh and spent **10CoCe** samples look nearly identical, further demonstrating the recoverable nature of the material.

Cerium $3d_{3/2,5/2}$ XPS spectra for the three mesoporous Co/CeO_2 catalysts are reported in Figure 3c. Ten peaks were fit to each spectrum and labeled according to Burroughs formalism. Each spectrum is composed of five spin−orbit split doublets (u: $3d_{3/2}$; v: $3d_{5/2}$) split by approximated 18.6 eV. For fitting purposes, the intensity ratio $I(3d_{5/2})/I(3d_{3/2})$ was fixed to 1.5 for each doublet pair.[44,45] All Ce $3d_{3/2,5/2}$ XPS spectra measured suggest a partially reduced CeO_2 material with the majority of cerium species in the Ce^{4+} oxidation state. An approximation of the degree of Ce^{4+} to Ce^{3+} reduction was obtained by calculating the percent composition of Ce^{3+} species using eq 1.

$$\%\ Ce^{3+} = \frac{A(u') + A(u0)}{A(u) + A(u') + A(u'') + A(u''') + A(u0)} \quad (1)$$

The Ce^{3+} content as a percentage of total cerium content was calculated to be 19%, 15%, and 18% for **1CoCe**, **5CoCe**, and **10CoCe**, respectively. The calculation detailed for **10CoCe** is reported in the Supporting Information in example 1 and eq S1. There are limitations of this calculation, which typically include a significant overestimation of Ce^{3+} content due to issues associated with X-ray irradiation, sample heating due to X-ray exposure, background fitting, and other quantification difficulties.[46,47] Additionally, since XPS is a surface-sensitive probe, these concentrations may not reflect bulk Ce^{3+} composition. Given these limitations, the cerium content in all three mesoporous Co/CeO_2 catalysts is partially reduced on the

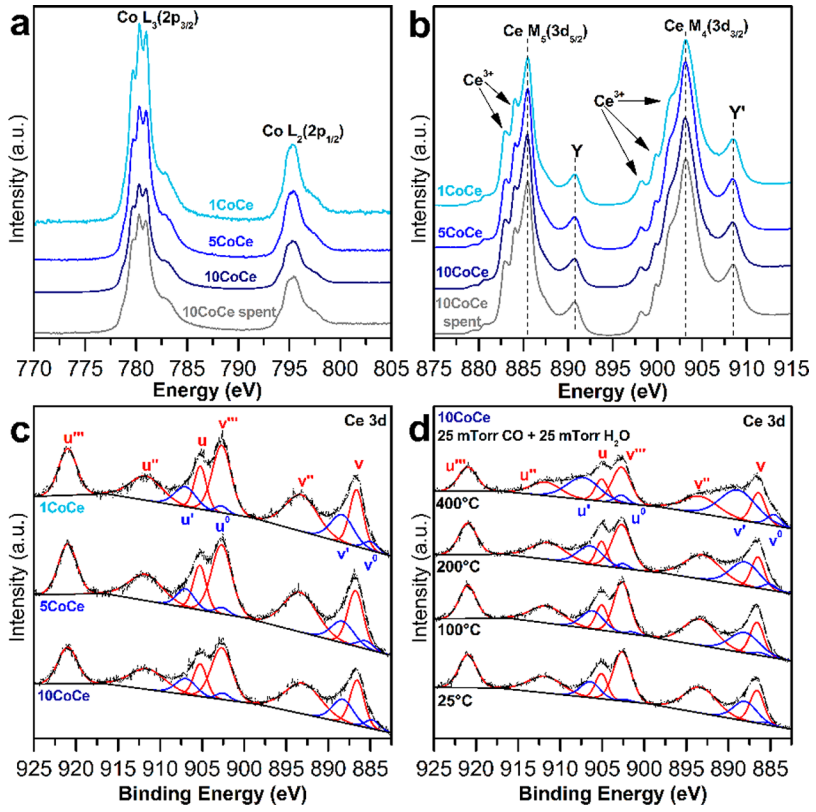

Figure 3. Spectroscopic study of mesoporous Co/CeO_2 materials: Co $L_{2,3}$ NEXAFS (a), Ce $M_{4,5}$ NEXAFS (b), Ce 3d XPS under vacuum conditions (c), and Ce 3d XPS of **10CoCe** under WGS ambient conditions (d).

DOI: 10.1021/acs.jpcc.8b01271
J. Phys. Chem. C 2018, 122, 8998−9008

surface without substantial difference with respect to cobalt loading.

Ambient pressure Ce $3d_{3/2,5/2}$ XPS measurements were conducted on the **10CoCe** sample in the presence of 25 mTorr of CO and 25 mTorr of H_2O to simulate water-gas shift reaction conditions (Figure 3d). The spectra at all temperature steps were fit and labeled as described previously, and eq 1 was used to approximate the Ce^{3+} concentration. Figure 4 reports

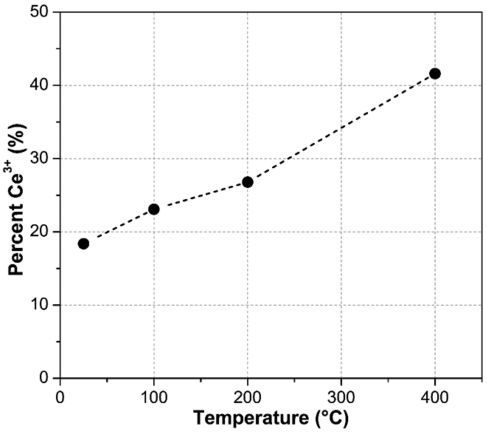

Figure 4. Ce^{3+} concentration as percentage of total cerium content in **10CoCe** calculated from XPS upon heating under ambient pressure WGS conditions.

the change of Ce^{3+} concentration with temperature under ambient pressure WGS conditions. Heating of the sample under these conditions resulted in an increase of Ce^{3+} composition from ~20% at room temperature to ~40% at 400 °C. This evident reduction of cerium in the CeO_2 lattice facilitates favorable catalytic properties due to the formation of additional oxygen vacancy sites that may serve as H_2O binding and splitting sites during the WGS reaction.[20] This CeO_2 surface reduction trend was observed in previous studies.[48]

Water-Gas Shift Catalytic Activity. The mesoporous Co/CeO_2 catalysts were evaluated for their activity for the high-temperature WGS reaction. The cobalt-containing catalysts were found to exhibit greater activity than the bare mesoporous CeO_2 material[24] by approximately 3 orders of magnitude when normalized by surface area (Figure 5a). This significant increase suggests that catalytic pathways involving cobalt are predominantly responsible for catalytic activity in these materials. Since the cobalt is likely highly dispersed with no evidence of phase segregation, activity was further normalized by the total nominal cobalt content (Figure 5b). The activity per unit cobalt was observed to decrease with increasing cobalt concentration. Furthermore, a significant deviation from linearity at higher temperatures was observed to intensify as cobalt content was increased and is most obvious for **10CoCe**. This deviation suggests catalyst deactivation at higher temperatures that is likely related to total cobalt content.

The WGS activity of **5CoCe** was also compared to a similarly prepared mesoporous 5% Cu/CeO_2 catalyst (**5CuCe**) that has been previously evaluated for its low-temperature WGS activity[25] (Figure 6). This comparison provides evidence for

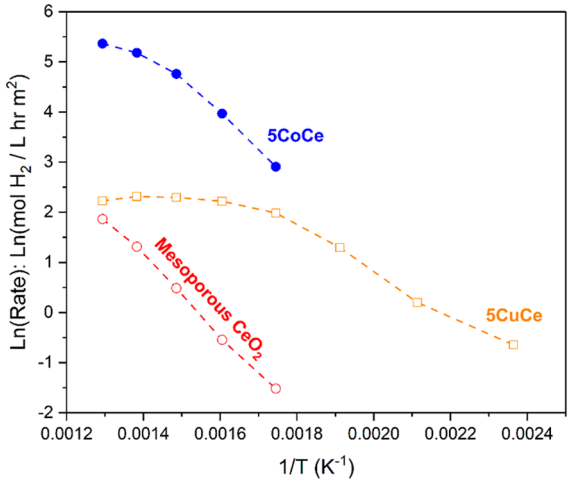

Figure 6. Activity plots for WGS catalytic activity over mesoporous copper and cobalt catalysts, normalized to surface area. Temperatures range from 500 °C ($1/T$ = 0.0013 K^{-1}) to 150 °C ($1/T$ = 0.002 36 K^{-1}) in 50 °C increments.

the superiority of the cobalt-loaded catalyst over copper at temperatures above approximately 300 °C. This trend is a consequence of metal−support interactions that determine the catalytic performance of the supported metals. When compared to bulk Cu, bulk Co is a poor WGS catalyst since it cleaves the C−O bond and catalyzes Fischer−Tropsch chemistry.

Active Bulk Structure. *In situ* synchrotron X-ray diffraction (XRD) was utilized in order to study the changes in the bulk

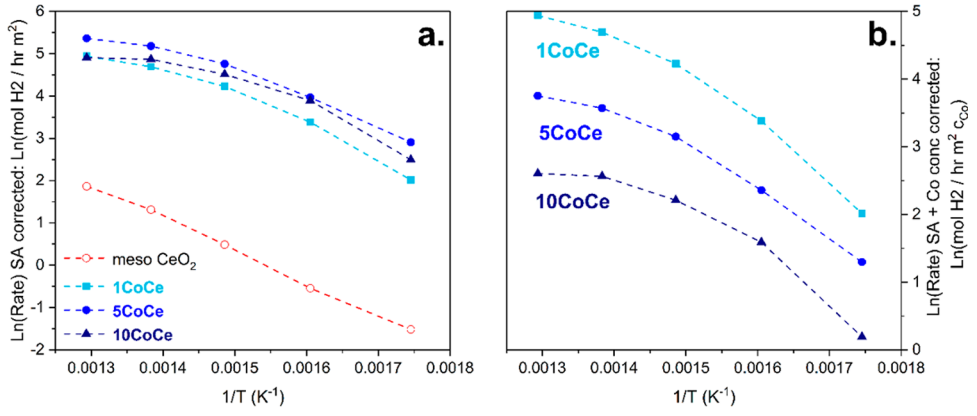

Figure 5. Activity plots for WGS catalytic activity over mesoporous catalysts normalized by surface area (a) and by surface area in addition to cobalt loading (b). Temperatures range from 500 °C ($1/T$ = 0.001 293 K^{-1}) to 300 °C ($1/T$ = 0.001 745 K^{-1}) in 50 °C increments.

DOI: 10.1021/acs.jpcc.8b01271
J. Phys. Chem. C 2018, 122, 8998−9008

crystalline structure of the mesoporous Co/CeO_2 catalysts as they were heated stepwise under WGS reactant gas flow (5% CO, 3% H_2O, balance He). Powder XRD patterns of **5CoCe** collected under these conditions are presented in Figure 7. Similar waterfall plots were prepared for **1CoCe** (Figure S4) and **10CoCe** (Figure S5) as well.

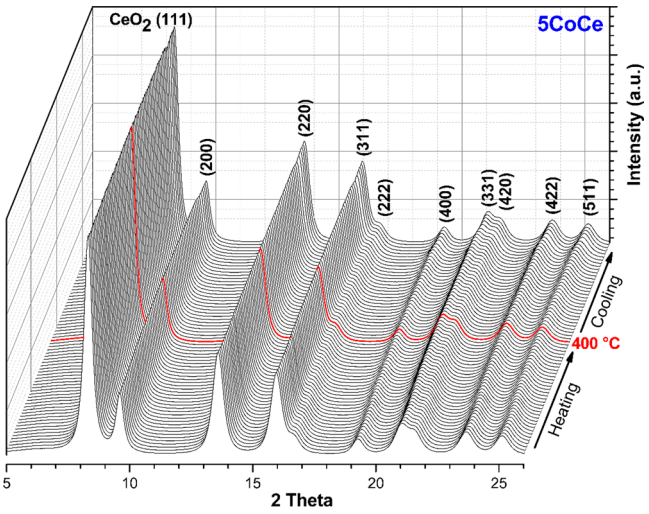

Figure 7. *In situ* X-ray diffraction patterns of **5CoCe** under WGS reaction conditions.

The CeO_2 fluorite type lattice was the sole crystalline phase observed over the course of all *in situ* XRD experiments. The absence of any segregated cobalt oxide or metal phase suggests that the Co/CeO_2 solid solution is robust under reaction conditions, although diffraction measurements do not rule out the presence of small segregated cobalt clusters with sizes below the diffraction limit or segregation of an amorphous phase.

The Rietveld method[35] was used to fit a model CeO_2 fluorite structure to each diffraction pattern. Using this refinement method, the average crystallite size was determined to be 6.2 nm for **1CoCe**, 6.8 nm for **5CoCe**, and 6.0 nm for **10CoCe**, which are slightly larger values than those determined by TEM. This sort of discrepancy is common since TEM is a highly localized technique, whereas XRD measurements represent an ensemble average of all exposed crystallites. The CeO_2 crystallite size remains stable without aggregation under reaction conditions.

The CeO_2 lattice parameters of bare mesoporous CeO_2 as well as mesoporous Co/CeO_2 catalysts over the course of the *in situ* XRD experiments are plotted in Figure 8. The absolute lattice parameter of cobalt-containing samples was observed to be significantly smaller than that of pure mesoporous CeO_2 at all temperatures, which may be attributed to the substitution of Ce^{4+} (r = 0.97 Å) with Co^{2+} (r = 0.65 Å) in the fluorite lattice.[49]

Upon heating the materials to 100 °C, a small contraction in the lattice was observed, likely related to the removal of precursor materials. Significant lattice expansion was observed for all samples upon heating between 100 and 250 °C. The cause for this expansion is most likely the reduction of Ce^{4+} (r = 0.97 Å) to Ce^{3+} (r = 1.14 Å) and formation of oxygen vacancies in the bulk of the CeO_2 material.[50,51] The shallow stepwise lattice expansion pattern visible at temperatures above approximately 250 °C is largely linear with temperature and is consistent with thermal expansion of cerium oxide.[52] This

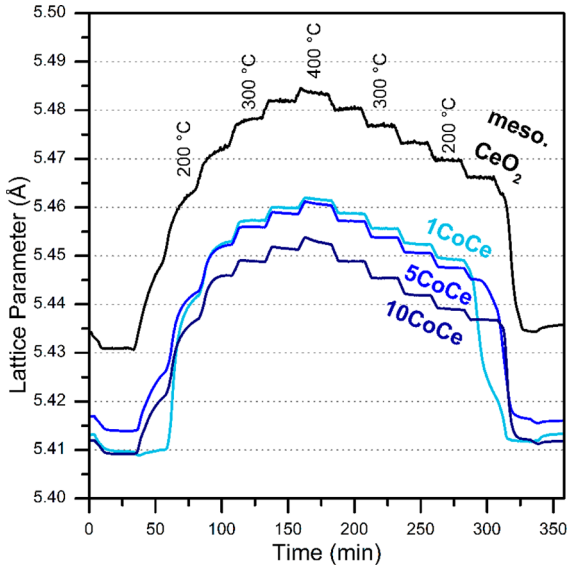

Figure 8. CeO_2 lattice parameters from Rietveld refinement of models fitted to *in situ* XRD data.

observation indicates that the majority of bulk cerium reduction takes place at temperatures below 300 °C. This result complements the surface-sensitive ambient pressure XPS data (Figure 4) that show a gentle increase of surface Ce^{3+} concentration from 100 to 200 °C, followed by more rapid reduction from 200 to 400 °C. In combination, these two data sets offer an insight into the complex surface vs bulk properties of these catalysts. Very likely, a stable equilibrium state for the bulk oxidation/reduction process occurs above approximately 200 °C, while a reversible change of the long-range bulk structure occurs below that temperature.

Relative bulk reducibility of catalyst materials was observed to vary with cobalt loading. In order to evaluate this reducibility factor, the minimum lattice parameter was subtracted from the maximum lattice parameter after the refinement analysis of each *in situ* XRD experiment. The resulting total lattice expansion was plotted against cobalt concentration in Figure 9. Since the thermal expansion component for each sample is nearly constant and significantly smaller than the component of lattice expansion due to cerium reduction, the total lattice expansion is analogous to the relative extent of bulk CeO_2 reducibility under WGS conditions. Using this metric, the

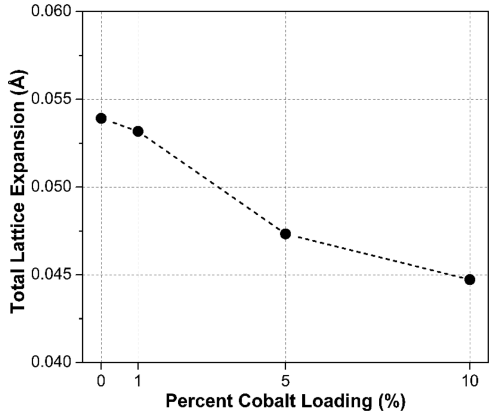

Figure 9. Total CeO_2 lattice expansion during *in situ* XRD experiments.

DOI: 10.1021/acs.jpcc.8b01271
J. Phys. Chem. C 2018, 122, 8998−9008

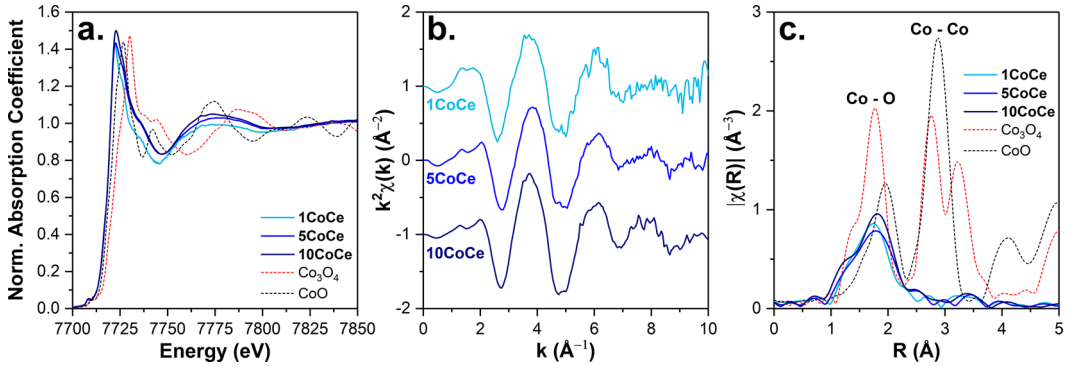

Figure 10. Co K-edge XANES (a) and k^2-weighed EXAFS data (b: in *k*-space; c: in *r*-space) for mesoporous Co/CeO_2 materials.

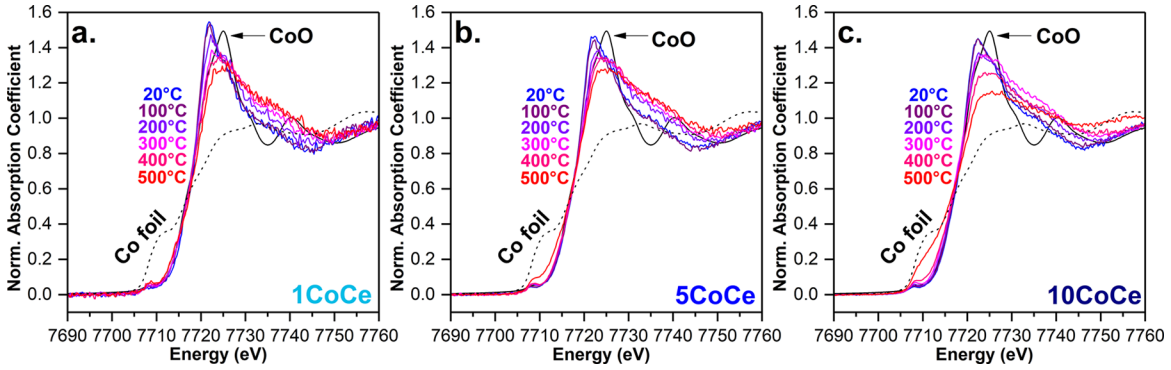

Figure 11. *In situ* Co K-edge XANES of **1CoCe** (a), **5CoCe** (b), and **10CoCe** (c) under water-gas shift reaction conditions.

introduction of cobalt into the mesoporous CeO_2 was observed to inhibit the reduction of cerium. Since cerium reduction is associated with the formation of catalytically important oxygen vacancy sites, increasing cobalt concentration likely creates an adverse effect on activity.

Cobalt Chemical State. Cobalt K-edge X-ray absorption measurements were conducted in order to elucidate the state and behavior of the cobalt content in the mesoporous Co/CeO_2 materials. Analysis of EXAFS data collected for fresh samples (Figure 10c) suggests that cobalt exists in an oxidized state, as evidenced by the short distance Co−O feature visible in the radial distribution function plot. The peak at approximately 1.8 Å is consistent with the Co−O peak measured for Co_3O_4 and is located at the shorter distance the Co−O peak measured for CoO. All features after approximately 2.5 Å are of very low intensity. Notably, the absence of any Co−Co features[53] rules out the presence of segregated cobalt oxide (or cobalt metal) phase in the fresh mesoporous Co/CeO_2 materials.

An examination of the state of cobalt under reaction conditions was carried out by measuring Co K-edge XANES while flowing WGS reactant gases (5% CO, 3% H_2O, balance He) and heating the samples. The resulting *in situ* XANES spectra are presented in Figure 11. Since the cobalt content in mesoporous Co/CeO_2 samples does not exist as any segregated oxide phase, the line shapes of the absorption spectra may not be attributed to a linear combination of oxide or metal standards. Nevertheless, metallic cobalt and CoO standards were included as reference materials for these measurements. Reliable EXAFS data were not obtained for samples under *in situ* conditions due to limitations associated with X-ray absorption by the quartz capillary as well as the highly absorbing cerium oxide content of the samples.

The notable components of the *in situ* XANES spectra include the position of the edge, the position of the white line, the intensity of the white line, and the nature of the pre-edge feature. Regardless of cobalt concentration, the room temperature intensity and position of the white line are indicative of an oxidized cobalt species. With increasing temperature, the intensity of the white line decreases and its position shifts to higher energy, a phenomenon typically associated with cobalt reduction. The extent of this change with temperature, however, differs with concentration. In **10CoCe**, the white line intensity is decreased significantly more at higher temperatures than that of **5CoCe** or **1CoCe**.

A small pre-edge feature around 7710 eV is visible in the room temperature XANES for all samples. In **1CoCe**, this feature remains approximately constant at all temperatures. In **5CoCe**, a change in the shape of this region is visible at 500 °C, when the pre-edge feature is observed to increase in intensity. This change is accompanied by a lower energy rise of the Co K edge. In **10CoCe**, this behavior is significantly more apparent. The increase in the pre-edge feature intensity and accompanying edge shift are observed at 400 °C and intensify as the sample is further heated to 500 °C. This pre-edge behavior is typically associated with the reduction of cobalt species to a metallic Co^0 state.[54]

In situ XANES results suggest that the cobalt content is reduced with increasing temperature under WGS reactant conditions. Increasing concentration of cobalt in the sample is associated with a greater degree of cobalt reduction. Small metallic clusters may have been formed at 400−500 °C, particularly in the **10CoCe** sample. The size of these clusters would need to be below the XRD detection limit,[55] however, as no metallic cobalt phase was observed during *in situ* X-ray diffraction experiments. Furthermore, the high-temperature

DOI: 10.1021/acs.jpcc.8b01271
J. Phys. Chem. C 2018, 122, 8998−9008

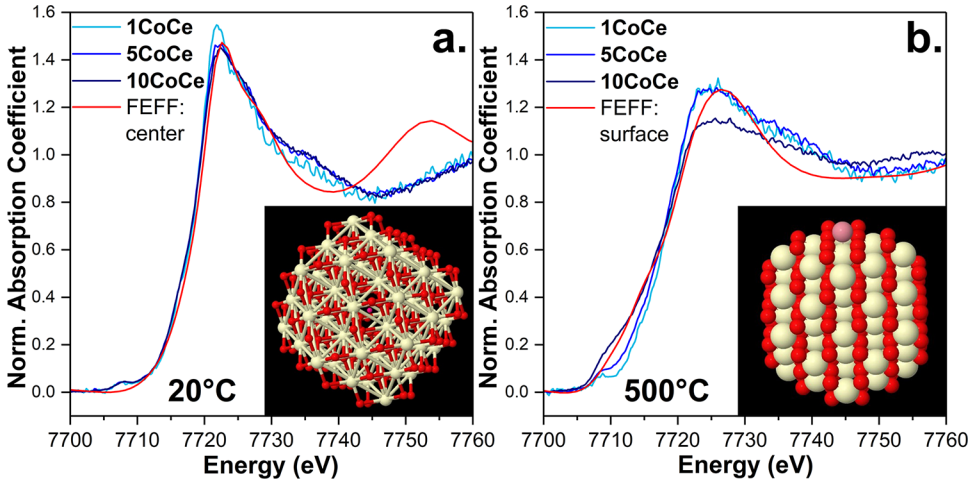

Figure 12. Co K-edge XANES FEFF 9 models of Co atom in center (a) and on top (b) of CeO_2 particle.

changes in the state of cobalt in **10CoCe** (and, to a lesser extent, **5CoCe**) may help explain the nonlinearity in the activity measurements at 400−500 °C (Figure 5). In correlation with XANES observations, the nonlinearity or downturn in activity is most obvious in **10CoCe** but is also present in **5CoCe** as well.

A negative causal relationship between the formation of small Co^0 metal clusters and catalytic activity would suggest that the active cobalt species is oxidized cobalt within the cerium oxide fluorite lattice. The CeO_2 lattice likely serves to stabilize cobalt in an oxidized state through favorable metal−support interactions, allowing this active species to exist in the highly reducing WGS reaction environment.

Co K-edge XANES data were also compared to two simulated XANES models of a cobalt atom sitting above of the surface layer and in the center of a ceria sphere. The simulated XANES spectrum from Co placed in the center of the CeO_2 particle resembles data collected for the three catalysts at room temperature (Figure 12a). The simulated spectrum from Co placed on top of the CeO_2 particle resembles data collected for the catalysts at 500 °C under reaction conditions (Figure 12b). It is possible that higher temperatures promote the mobility of cobalt from the center to the surface of CeO_2 under WGS conditions. With higher cobalt concentrations, this mobility could cause aggregation of cobalt atoms at the surface and subsequent formation of inactive cobalt clusters.

***In Situ* Surface Chemistry.** *In situ* infrared spectroscopy (DRIFTS) was used to examine chemical species present on the surface of the mesoporous Co/CeO_2 catalysts under WGS reaction conditions. Representative DRIFTS spectra collected for **5CoCe** are plotted in Figure 13. Similar plots were prepared for **1CoCe** (Figure S6) and **10CoCe** (Figure S7). At room temperature, a broad feature around 3300 cm^{-1} indicates the presence of water, and another feature at 1635 cm^{-1} corresponds to water that has been molecularly adsorbed onto the catalyst surface.[56] As the temperature is increased, these features are removed and are replaced with smaller peaks around 3600 cm^{-1} that correspond to hydroxyl species on cerium oxide.[57,58] These hydroxyl species are formed following the dissociation of H_2O as a part of the WGS reaction. Around 150 °C, the development of several peaks between 3000 and 2500 cm^{-1} is evident. The three peaks at 2932, 2842, and 2721 cm^{-1} correspond to δ(C−H) + ν_s(OCO), ν(C−H), and 2δ(C−H) of bidentate formate on CeO_2, respectively.[57,59]

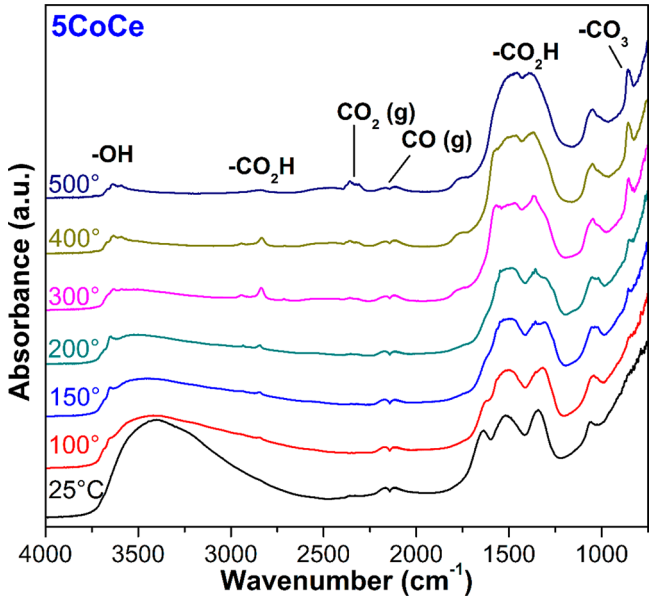

Figure 13. DRIFTS of **5CoCe** under WGS reaction conditions.

Additional formate peaks are present in the region between 1750 and 1250 cm^{-1}, but this area is difficult to deconvolute. A feature at around 855 cm^{-1} also develops around 150 °C, which may correspond to various configurations of carbonate species on the CeO_2 surface.[59]

As the temperature is increased to the catalytically active conditions between 300 and 500 °C, a gas phase CO_2 feature is evident, indicating WGS catalytic activity. Furthermore, the bidentate formate features decrease in intensity as this species becomes labile on the catalyst surface. The carbonate feature continues to increase with temperature, however. This behavior was documented on bare mesoporous CeO_2 as well[24] and may be attributed to the affinity of CeO_2 (100) surfaces for strongly binding tridentate carbonate.[60]

A comparison of DRIFTS spectra for the studied catalyst materials at 400 °C is presented in Figure 14. The intensity of features associated with surface hydroxyl species is observed to decrease as cobalt concentration increases. This observation corroborates our *in situ* X-ray diffraction experiments, which suggest a decrease in oxygen vacancy sites (H_2O splitting sites) with increasing cobalt concentration (Figure 9). The intensity

DOI: 10.1021/acs.jpcc.8b01271
J. Phys. Chem. C 2018, 122, 8998−9008

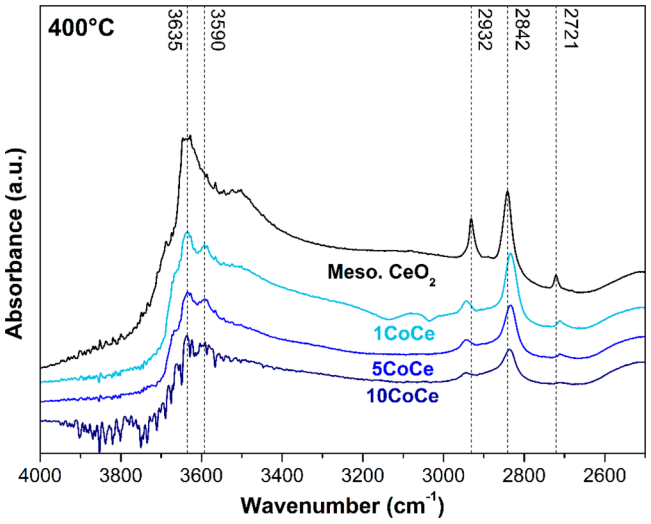

Figure 14. DRIFTS of catalyst materials under WGS reaction conditions at 400 °C.

of bands associated with bidentate formate also decreases with increasing cobalt concentration. Formate species have been previously identified as potential intermediates[24] in the associative pathway[22] for the WGS reaction over bare mesoporous CeO_2. This pathway accounts for a greater portion of catalytic activity over catalysts with smaller cobalt loading.

CONCLUSION

Following the development of a novel and catalytically active mesoporous morphology of cerium oxide, we have synthesized, tested, and characterized mesoporous Co/CeO_2 catalysts with varying cobalt concentrations (**1CoCe**, **5CoCe**, and **10CoCe**). Morphological examination of the material revealed a mesoporous structure consisting of highly crystalline and monodisperse nanoparticles with a fluorite type structure similar to CeO_2. Cobalt was observed by EDX to be present in concentrations in agreement with nominal loadings and well dispersed within the materials. Imaging, scattering, and spectroscopic techniques did not reveal evidence of any segregated cobalt or cobalt oxide phase, suggesting that cobalt exists primarily in a solid solution state within the ceria lattice. This solid solution has special catalytic properties with respect to metallic cobalt.

The mesoporous Co/CeO_2 catalysts were found to be active for water-gas shift reaction in the 300−500 °C temperature range. When normalized by cobalt content, the lowest loading (**1CoCe**) exhibited greatest activity per unit cobalt. Under reaction conditions, reduction of surface and bulk cerium was observed as well as partial reduction of the cobalt content. Catalysts with higher cobalt loadings (**5CoCe** and to a greater extent **10CoCe**) were found to exhibit deactivation behavior at temperatures above 400 °C, possibly related to the segregation of very small clusters of metallic cobalt. *In situ* XRD and DRIFTS experiments suggest a more facile formation of active oxygen vacancy sites on catalysts with lower cobalt loadings, particularly **1CoCe**, providing a likely explanation for enhanced activity. Additional associative pathways may also be present, as evidenced by the DRIFTS observations of carbonaceous surface species under WGS reaction conditions.

The reaction environment characterization of these low cobalt loading catalysts is a part of an ongoing effort to foster an understanding of the structural, chemical, and mechanistic properties of catalytic materials for industrially important reactions like the water-gas shift. The strong interactions seen between mesoporous ceria and cobalt may aid in the development of new and inexpensive catalysts through evidence-based material design and synthesis.

ASSOCIATED CONTENT

Supporting Information

The Supporting Information is available free of charge on the ACS Publications website at DOI: 10.1021/acs.jpcc.8b01271.

Figures S1−S7: additional microscopy, X-ray diffraction, and infrared spectroscopy data; an example of an XPS quantification based on eq 1 (PDF)

AUTHOR INFORMATION

Corresponding Authors

*E-mail Steven.suib@uconn.edu; Ph 631-344-4343 (S.L.S.).
*E-mail ssenanay@bnl.gov (S.D.S.).

ORCID

Dimitriy Vovchok: 0000-0001-6423-7566
Jordi Llorca: 0000-0002-7447-9582
Zongyuan Liu: 0000-0001-8526-5590
Iradwikanari Waluyo: 0000-0002-4046-9722
Anatoly I. Frenkel: 0000-0002-5451-1207
José A. Rodriguez: 0000-0002-5680-4214
Steven L. Suib: 0000-0003-3073-311X
Sanjaya D. Senanayake: 0000-0003-3991-4232

Notes

The authors declare no competing financial interest.

ACKNOWLEDGMENTS

The research carried out at Brookhaven National Laboratory was supported by the U.S. Department of Energy, Office of Science and Office of Basic Energy Sciences under Contract No. DE-SC0012704. S.D.S is also supported by a U.S. Department of Energy Early Career Award. This research used resources of the 8-ID (ISS) and 23-ID-2 (IOS) beamlines of the National Synchrotron Light Source II, a U.S. Department of Energy (DOE) Office of Science User Facility operated for the DOE Office of Science by Brookhaven National Laboratory under Contract No. DE-SC0012704. This work also used resources of the Advanced Photon Source (17B-M), a U.S. Department of Energy (DOE) Office of Science User Facility operated for the DOE Office of Science by Argonne National Laboratory under Contract No. DE-AC02-06CH11357. J.L. is a Serra Hunter Fellow and is grateful to the ICREA Academia Program and MINECO/FEDER Grant ENE2015-63969-R and GC 2017 SGR 128. S.L.S. acknowledges support from the U.S. Department of Energy, Office of Basic Energy Sciences, Division of Chemical, Biological and Geological Sciences (Grant DE-FG02-86ER13622A00) as well as the assistance of the Bioscience Electron Microscopy Laboratory of the University of Connecticut and Grant # 1126100 for the purchase of the FEI NovaSEM. A.I.F. acknowledges support from the U.S. Department of Energy, Office of Basic Energy Sciences Division of Chemical, Biological and Geological Sciences (Grant DE-FG02-03ER15476). The authors also acknowledge Dr. Taejin Kim and Mr. Xiaojun Chan from Stony Brook University for making available their infrared spectroscopy facilities for the purposes of this work.

DOI: 10.1021/acs.jpcc.8b01271
J. Phys. Chem. C 2018, 122, 8998−9008

REFERENCES

(1) Dincer, I.; Acar, C. Review and Evaluation of Hydrogen Production Methods for Better Sustainability. *Int. J. Hydrogen Energy* **2015**, *40*, 11094−11111.
(2) Hickman, D. A.; Schmidt, L. D. Production of Syngas by Direct Catalytic Oxidation of Methane. *Science* **1993**, *259*, 343−346.
(3) Li, Q.; He, R.; Gao, J.-A.; Jensen, J. O.; Bjerrum, N. J. The Co Poisoning Effect in Pemfcs Operational at Temperatures up to 200°C. *J. Electrochem. Soc.* **2003**, *150*, A1599−A1605.
(4) Newsome, D. S. The Water-Gas Shift Reaction. *Catal. Rev.: Sci. Eng.* **1980**, *21*, 275−318.
(5) Batista, M. S.; Santiago, E. I.; Assaf, E. M.; Ticianelli, E. A. Evaluation of the Water-Gas Shift and Co Methanation Processes for Purification of Reformate Gases and the Coupling to a Pem Fuel Cell System. *J. Power Sources* **2005**, *145*, 50−54.
(6) Kolb, G.; Schurer, J.; Tiemann, D.; Wichert, M.; Zapf, R.; Hessel, V.; Lowe, H. Fuel Processing in Integrated Micro-Structured Heat-Exchanger Reactors. *J. Power Sources* **2007**, *171*, 198−204.
(7) Spivey, J. J. Catalysis in the Development of Clean Energy Technologies. *Catal. Today* **2005**, *100*, 171−180.
(8) Sun, Y.; Hla, S. S.; Duffy, G. J.; Cousins, A. J.; French, D.; Morpeth, L. D.; Edwards, J. H.; Roberts, D. G. Effect of Ce on the Structural Features and Catalytic Properties of La(0.9−X)Cexfeo3 Perovskite-Like Catalysts for the High Temperature Water−Gas Shift Reaction. *Int. J. Hydrogen Energy* **2011**, *36*, 79−86.
(9) Keiski, R. L.; Salmi, T.; Niemistö, P.; Ainassaari, J.; Pohjola, V. J. Stationary and Transient Kinetics of the High Temperature Water-Gas Shift Reaction. *Appl. Catal., A* **1996**, *137*, 349−370.
(10) Salmi, T.; Boström, S.; Lindfors, L. E. A Dynamic Study of the Water-Gas Shift Reaction over an Industrial Ferrochrome Catalyst. *J. Catal.* **1988**, *112*, 345−356.
(11) Zhu, M.; Wachs, I. E. Iron-Based Catalysts for the High-Temperature Water−Gas Shift (Ht-Wgs) Reaction: A Review. *ACS Catal.* **2016**, *6*, 722−732.
(12) Meshkani, F.; Rezaei, M. High Temperature Water Gas Shift Reaction over Promoted Iron Based Catalysts Prepared by Pyrolysis Method. *Int. J. Hydrogen Energy* **2014**, *39*, 16318−16328.
(13) Fu, Q.; Saltsburg, H.; Flytzani-Stephanopoulos, M. Active Nonmetallic Au and Pt Species on Ceria-Based Water-Gas Shift Catalysts. *Science* **2003**, *301*, 935−938.
(14) Hilaire, S.; Wang, X.; Luo, T.; Gorte, R. J.; Wagner, J. A Comparative Study of Water-Gas-Shift Reaction over Ceria Supported Metallic Catalysts. *Appl. Catal., A* **2001**, *215*, 271−278.
(15) Li, Y.; Fu, Q.; Flytzani-Stephanopoulos, M. Low-Temperature Water-Gas Shift Reaction over Cu- and Ni-Loaded Cerium Oxide Catalysts. *Appl. Catal., B* **2000**, *27*, 179−191.
(16) Si, R.; Flytzani-Stephanopoulos, M. Shape and Crystal-Plane Effects of Nanoscale Ceria on the Activity of Au-Ceo2 Catalysts for the Water−Gas Shift Reaction. *Angew. Chem., Int. Ed.* **2008**, *47*, 2884−2887.
(17) Chueh, W. C.; Falter, C.; Abbott, M.; Scipio, D.; Furler, P.; Haile, S. M.; Steinfeld, A. High-Flux Solar-Driven Thermochemical Dissociation of Co2 and H2o Using Nonstoichiometric Ceria. *Science* **2010**, *330*, 1797−1801.
(18) Mullins, D. R. The Surface Chemistry of Cerium Oxide. *Surf. Sci. Rep.* **2015**, *70*, 42−85.
(19) Farmer, J. A.; Campbell, C. T. Ceria Maintains Smaller Metal Catalyst Particles by Strong Metal-Support Bonding. *Science* **2010**, *329*, 933−936.
(20) Hansen, H. A.; Wolverton, C. Kinetics and Thermodynamics of H2o Dissociation on Reduced Ceo2(111). *J. Phys. Chem. C* **2014**, *118*, 27402−27414.
(21) Putna, E. S.; Vohs, J. M.; Gorte, R. J. Evidence for Weakly Bound Oxygen on Ceria Films. *J. Phys. Chem.* **1996**, *100*, 17862−17865.
(22) Rodriguez, J. A.; Liu, P.; Hrbek, J.; Evans, J.; Pérez, M. Water Gas Shift Reaction on Cu and Au Nanoparticles Supported on Ceo2(111) and Zno(000−1): Intrinsic Activity and Importance of Support Interactions. *Angew. Chem., Int. Ed.* **2007**, *46*, 1329−1332.
(23) Poyraz, A. S.; Kuo, C.-H.; Biswas, S.; King'ondu, C. K.; Suib, S. L. A General Approach to Crystalline and Monomodal Pore Size Mesoporous Materials. *Nat. Commun.* **2013**, *4*, 2952.
(24) Guild, C. J.; et al. Water-Gas-Shift over Metal-Free Nanocrystalline Ceria: An Experimental and Theoretical Study. *ChemCatChem* **2017**, *9*, 1373−1377.
(25) Vovchok, D. Cu Supported on Mesoporous Ceria: Water Gas Shift Activity at Low Cu Loadings through Metal-Support Interactions. *Phys. Chem. Chem. Phys.* **2017**, *19*, 17708.
(26) Jha, A.; Jeong, D.-W.; Lee, Y.-L.; Nah, I. W.; Roh, H.-S. Enhancing the Catalytic Performance of Cobalt Oxide by Doping on Ceria in the High Temperature Water-Gas Shift Reaction. *RSC Adv.* **2015**, *5*, 103023−103029.
(27) Lee, Y.-L.; et al. Optimization of Cobalt Loading in Co−Ceo2 Catalyst for the High Temperature Water−Gas Shift Reaction. *Top. Catal.* **2017**, *60*, 721−726.
(28) Xie, X.; Li, Y.; Liu, Z.-Q.; Haruta, M.; Shen, W. Low-Temperature Oxidation of Co Catalysed by Co3o4 Nanorods. *Nature* **2009**, *458*, 746.
(29) Majima, T.; Kono, E.; Ogo, S.; Sekine, Y. Pre-Reduction and K Loading Effects on Noble Metal Free Co-System Catalyst for Water Gas Shift Reaction. *Appl. Catal., A* **2016**, *523*, 92−96.
(30) Xie, X.; Yin, H.; Dou, B.; Huo, J. Characterization of a Potassium-Promoted Cobalt- Molybdenum/Alumina Water-Gas Shift Catalyst. *Appl. Catal.* **1991**, *77*, 187−198.
(31) Nagai, M.; Matsuda, K. Low-Temperature Water−Gas Shift Reaction over Cobalt−Molybdenum Carbide Catalyst. *J. Catal.* **2006**, *238*, 489−496.
(32) Fairley, N.; Ltd., C. S. Casaxps Manual 2.3.15: Casaxpx Processing Software for Xps Spectra; Casa Software Limited, 2009.
(33) Chupas, P. J.; Chapman, K. W.; Kurtz, C.; Hanson, J. C.; Lee, P. L.; Grey, C. P. A Versatile Sample-Environment Cell for Non-Ambient X-Ray Scattering Experiments. *J. Appl. Crystallogr.* **2008**, *41*, 822−824.
(34) Toby, B. H.; Von Dreele, R. B. Gsas-Ii: The Genesis of a Modern Open-Source All Purpose Crystallography Software Package. *J. Appl. Crystallogr.* **2013**, *46*, 544−549.
(35) Albinati, A.; Willis, B. T. M. The Rietveld Method in Neutron and X-Ray Powder Diffraction. *J. Appl. Crystallogr.* **1982**, *15*, 361−374.
(36) Ravel, B.; Newville, M. Athena, Artemis, Hephaestus: Data Analysis for X-Ray Absorption Spectroscopy Using Ifeffit. *J. Synchrotron Radiat.* **2005**, *12*, 537−41.
(37) Rehr, J. J.; Kas, J. J.; Vila, F. D.; Prange, M. P.; Jorissen, K. Parameter-Free Calculations of X-Ray Spectra with Feff9. *Phys. Chem. Chem. Phys.* **2010**, *12*, 5503−5513.
(38) Deshpande, S.; Patil, S.; Kuchibhatla, S. V.; Seal, S. Size Dependency Variation in Lattice Parameter and Valency States in Nanocrystalline Cerium Oxide. *Appl. Phys. Lett.* **2005**, *87*, 133113.
(39) Brunauer, S.; Emmett, P. H.; Teller, E. Adsorption of Gases in Multimolecular Layers. *J. Am. Chem. Soc.* **1938**, *60*, 309−319.
(40) Istomin, S. Y.; et al. An Unusual High-Spin Ground State of Co3+ in Octahedral Coordination in Brownmillerite-Type Cobalt Oxide. *Dalton Transactions* **2015**, *44*, 10708−10713.
(41) Lin, H. J.; et al. Local Orbital Occupation and Energy Levels of Co in Naxcoo2: A Soft X-Ray Absorption Study. *Phys. Rev. B: Condens. Matter Mater. Phys.* **2010**, *81*, 115138.
(42) Wang, J.; Zhou, J.; Hu, Y.; Regier, T. Chemical Interaction and Imaging of Single Co3o4/Graphene Sheets Studied by Scanning Transmission X-Ray Microscopy and X-Ray Absorption Spectroscopy. *Energy Environ. Sci.* **2013**, *6*, 926−934.
(43) Smythe, D. J.; Brenan, J. M.; Bennett, N. R.; Regier, T.; Henderson, G. S. Quantitative Determination of Cerium Oxidation States in Alkali-Aluminosilicate Glasses Using M4,5-Edge Xanes. *J. Non-Cryst. Solids* **2013**, *378*, 258−264.
(44) Bêche, E.; Charvin, P.; Perarnau, D.; Abanades, S.; Flamant, G. Ce 3d Xps Investigation of Cerium Oxides and Mixed Cerium Oxide (Cextiyoz). *Surf. Interface Anal.* **2008**, *40*, 264−267.
(45) Paparazzo, E. On the Curve-Fitting of Xps Ce(3d) Spectra of Cerium Oxides. *Mater. Res. Bull.* **2011**, *46*, 323−326.

DOI: 10.1021/acs.jpcc.8b01271
J. Phys. Chem. C 2018, 122, 8998−9008

(46) Chen, L.; Fleming, P.; Morris, V.; Holmes, J. D.; Morris, M. A. Size-Related Lattice Parameter Changes and Surface Defects in Ceria Nanocrystals. *J. Phys. Chem. C* **2010**, *114*, 12909−12919.
(47) Zhang, F.; Wang, P.; Koberstein, J.; Khalid, S.; Chan, S. W. Cerium Oxidation State in Ceria Nanoparticles Studied with X-Ray Photoelectron Spectroscopy and Absorption near Edge Spectroscopy. *Surf. Sci.* **2004**, *563*, 74−82.
(48) Reina, T. R.; Xu, W. Q.; Ivanova, S.; Centeno, M. A.; Hanson, J.; Rodriguez, J. A.; Odriozola, J. A. In Situ Characterization of Iron-Promoted Ceria-Alumina Gold Catalysts During the Water-Gas Shift Reaction. *Catal. Today* **2013**, *205*, 41−48.
(49) Ansari, A. A.; Labis, J.; Alam, M.; Ramay, S. M.; Ahmad, N.; Mahmood, A. Effect of Cobalt Doping on Structural, Optical and Redox Properties Cerium Oxide Nanoparticles. *Phase Transitions* **2016**, *89*, 261−272.
(50) Xu, W. Q.; Si, R.; Senanayake, S. D.; Llorca, J.; Idriss, H.; Stacchiola, D.; Hanson, J. C.; Rodriguez, J. A. In Situ Studies of Ceo2-Supported Pt, Ru, and Pt-Ru Alloy Catalysts for the Water-Gas Shift Reaction: Active Phases and Reaction Intermediates. *J. Catal.* **2012**, *291*, 117−126.
(51) Wang, X.; Rodriguez, J. A.; Hanson, J. C.; Gamarra, D.; Martínez-Arias, A.; Fernández-García, M. In Situ Studies of the Active Sites for the Water Gas Shift Reaction over Cu−Ceo2 Catalysts: Complex Interaction between Metallic Copper and Oxygen Vacancies of Ceria. *J. Phys. Chem. B* **2006**, *110*, 428−434.
(52) Trovarelli, A. Catalytic Properties of Ceria and Ceo2-Containing Materials. *Catal. Rev.: Sci. Eng.* **1996**, *38*, 439−520.
(53) Rosen, J.; Hutchings, G. S.; Jiao, F. Synthesis, Structure, and Photocatalytic Properties of Ordered Mesoporous Metal-Doped Co3o4. *J. Catal.* **2014**, *310*, 2−9.
(54) Jacobs, G.; Williams, L.; Graham, U.; Sparks, D.; Davis, B. H. Low-Temperature Water-Gas Shift: In-Situ Drifts−Reaction Study of a Pt/Ceo2 Catalyst for Fuel Cell Reformer Applications. *J. Phys. Chem. B* **2003**, *107*, 10398−10404.
(55) Frenkel, A. I.; Wang, Q.; Marinkovic, N.; Chen, J. G.; Barrio, L.; Si, R.; Cámara, A. L.; Estrella, A. M.; Rodriguez, J. A.; Hanson, J. C. Combining X-Ray Absorption and X-Ray Diffraction Techniques for in Situ Studies of Chemical Transformations in Heterogeneous Catalysis: Advantages and Limitations. *J. Phys. Chem. C* **2011**, *115*, 17884−17890.
(56) Zhao, F.; et al. Water-Gas Shift Reaction on Ni−W−Ce Catalysts: Catalytic Activity and Structural Characterization. *J. Phys. Chem. C* **2014**, *118*, 2528−2538.
(57) Binet, C.; Daturi, M.; Lavalley, J. C. Ir Study of Polycrystalline Ceria Properties in Oxidised and Reduced States. *Catal. Today* **1999**, *50*, 207−225.
(58) Yao, S. Y.; Xu, W. Q.; Johnston-Peck, A. C.; Zhao, F. Z.; Liu, Z. Y.; Luo, S.; Senanayake, S. D.; Martinez-Arias, A.; Liu, W. J.; Rodriguez, J. A. Morphological Effects of the Nanostructured Ceria Support on the Activity and Stability of Cuo/Ceo2 Catalysts for the Water-Gas Shift Reaction. *Phys. Chem. Chem. Phys.* **2014**, *16*, 17183−95.
(59) Vayssilov, G. N.; Mihaylov, M.; Petkov, P. S.; Hadjiivanov, K. I.; Neyman, K. M. Reassignment of the Vibrational Spectra of Carbonates, Formates, and Related Surface Species on Ceria: A Combined Density Functional and Infrared Spectroscopy Investigation. *J. Phys. Chem. C* **2011**, *115*, 23435−23454.
(60) Albrecht, P. M.; Jiang, D.-e.; Mullins, D. R. Co2 Adsorption as a Flat-Lying, Tridentate Carbonate on Ceo2(100). *J. Phys. Chem. C* **2014**, *118*, 9042−9050.

DOI: 10.1021/acs.jpcc.8b01271
J. Phys. Chem. C 2018, 122, 8998−9008